

Original article

Theoretical study of structural stability and electronic properties of $\text{Sr}_2\text{MnSbO}_6$ perovskite

Estudio teórico de la estabilidad estructural y propiedades electrónicas de la perovskita $\text{Sr}_2\text{MnSbO}_6$

William Oswaldo Sosa-Correa^{1,*}, Luis Fernando Muñoz-Martínez²,

José Otálora-Acevedo¹, Jairo Roa-Rojas³, Jairo Arbey Rodríguez⁴

¹ Escuela de Física, Universidad Pedagógica y Tecnológica de Colombia, Tunja, Colombia

² Departamento de Ciencias Básicas, Universidad del Sinú, Montería, Córdoba, Colombia

³ Grupo de Física de Nuevos Materiales - GFNM, Departamento de Física, Universidad Nacional de Colombia, Bogotá, Colombia

⁴ Grupo de Estudio de Materiales - GEMA, Departamento de Física, Universidad Nacional de Colombia, Bogotá, Colombia

Abstract

Structural and electronic properties of the $\text{Sr}_2\text{MnSbO}_6$ perovskite in cubic (Fm-3m) and tetragonal (I4m and P/4mnc) crystallographic phases have been determined using the Full Potential Linearized Augmented Plane Waves (FP-LAPW) method, in the framework of the Density Functional Theory (DFT). The exchange and correlation effects were treated using the Generalized Gradient Approximation plus the Hubbard term (GGA+U) approach, in order to describe the strong on-site Coulomb repulsion among the localized d-Mn electrons. The structural stability was determined by fitting of the total energy values to the Murnaghan equation of state. The values for the structural parameters are in good agreement with experimental results reported in the literature. The study of the electronic properties carried out through the graphical presentation of the densities of states for the two spin polarizations shows that the compound presents half-metallic behavior.

Keywords: Double perovskite; $\text{Sr}_2\text{MnSbO}_6$; Half-Metallicity; Density of States.

Resumen

Las propiedades estructurales y electrónicas de la perovskita $\text{Sr}_2\text{MnSbO}_6$ en sus fases cúbica (Fm-3m) y tetragonales (I4m y P/4mnc) han sido determinadas usando el método de Ondas Planas Aumentadas y Linealizadas con potencial completo (FP-LAPW), dentro del formalismo de la Teoría del Funcional de la Densidad (DFT). Los efectos de intercambio y correlación fueron tratados usando la aproximación de Gradiente Generalizado e incluyendo el termino de Hubbard (GGA+U), con el objeto de describir la fuerte repulsión electrónica in situ entre los electrones d-Mn localizados. La estabilidad estructural fue determinada ajustando los valores para la energía total, a la ecuación de estado de Murnaghan. Los valores para los parámetros estructurales están de acuerdo con resultados experimentales reportados en la literatura. El estudio de las propiedades electrónicas realizado mediante la representación de las densidades de estados para las dos polarizaciones de espín, muestra que el compuesto presenta un comportamiento semimetálico.

Palabras clave: Perovskita doble; $\text{Sr}_2\text{MnSbO}_6$; semimetalicidad; Densidades de estados.

Citation: Sosa-Correa WO, Muñoz-Martínez LF, Otálora-Acevedo J, *et al.* Theoretical study of structural stability and electronic properties of $\text{Sr}_2\text{MnSbO}_6$ perovskite. *Revista de la Academia Colombiana de Ciencias Exactas, Físicas y Naturales.* 47(182):72-80, enero-marzo de 2023. doi: <https://doi.org/10.18257/raccefyn.1801>

Editor: Rafael González Hernández

***Corresponding autor:**

William Sosa Correa;
wosecydm@gmail.com

Received: November 1, 2022

Accepted: January 17, 2023

Published on line: February 6, 2023



This is an open access article distributed under the terms of the Creative Commons Attribution License.

Introduction

In recent years the magneto-electric compounds have attracted scientific and technological interest in science community, because they represent very interesting potential applications in electronic devices. Into this family of compounds are the complex perovskite oxides of $\text{A}_2\text{MM}'\text{O}_6$ kind, where A is an alkaline earth and M, M' are magnetic and non-magnetic

transition metal, respectively. The Sr₂MnSbO₆ perovskite is one compound of this type, and it has been synthesized via molten salt synthesis (MSS) method and convectional solid-state methods for example by (Cheah *et al.*, 2006; Ivanov *et al.*, 2009; Parada *et al.*, 2018; Preethi-Meher *et al.*, 2012). Experimental studies of Sr₂MnSbO₆ have shown that this compound presents ferroelectric and ferromagnetic behavior in the I4m, I4mm, I4mcm phases, as well as it exhibits high dielectric constant in the cubic phase Fm-3m (Antara, *et al.*, 2011; Foster, *et al.*, 1997; Majhi & Varma, 2007). Modifications of this compound recently have been reported by (Bazuev *et al.*, 2021), where is studied the effect of substitutions on the phase formation, structure and magnetic properties of the Sr₂MnSbO₆ compound.

The theoretical study of the A₂MM'O₆ compounds is usually tackled using the DFT framework. Its useful accuracy and low computational cost made DFT the main tool in the prediction of properties of materials. In particular, the study of complex perovskite oxides involves effects to take in account, such as the strong correlation between electrons of the transition metals elements, which are included into the DFT formalism. For example, theoretical calculations of the Sr₂MnSbO₆ compound using DFT framework in its pseudopotential approach (Singh & Nordstrom, 2006) with GGA+U approximation are reported in (Persson, 2016), for the tetragonal space group I4/mmm. This phase is reported as semiconductor with band gap equal to 0.208 eV, and effective magnetic moment 4.0 μ_B . Moreover, DFT in the FP-LAPW version is applied in a broad range of the A₂MM'O₆ kind compounds by (Mir & Gupta, 2020; Bonilla *et al.*, 2007; Cardona *et al.*, 2008; Fajardo *et al.*, 2012; Liu, *et al.*, 2014; Mir & Gupta, 2021; Ortiz-Diaz *et al.*, 2007), where are included transition metals such as Cr, Co, Fe, Ni, Mn, among others. In the above mentioned cases, those complex perovskites present the so-called half-metallic behavior. This exotic property is characterized because the material has completely polarized spin states at the Fermi level, allowing the conduction of charge with specific spin (up or down). Such behavior makes these materials candidates for applications in spintronics as sources of unique spin and high efficiency sensors.

The success of the density functional theory methods to compute properties of materials like the complex perovskite oxides, lead us to develop theoretical calculations based on density functional theory (DFT), aiming to elucidate the properties of the Sr₂MnSbO₆ perovskite. The theoretical calculations performed here show that all, cubic (Fm-3m) and tetragonal phases (I4m and P4/mnc), are stable phases of this compound. Our findings agree with different experimental reports of the structural parameters. In addition, in this paper we present calculations of densities of states (DOS), through which a half-metallic behavior in the cubic and tetragonal structures is demonstrated.

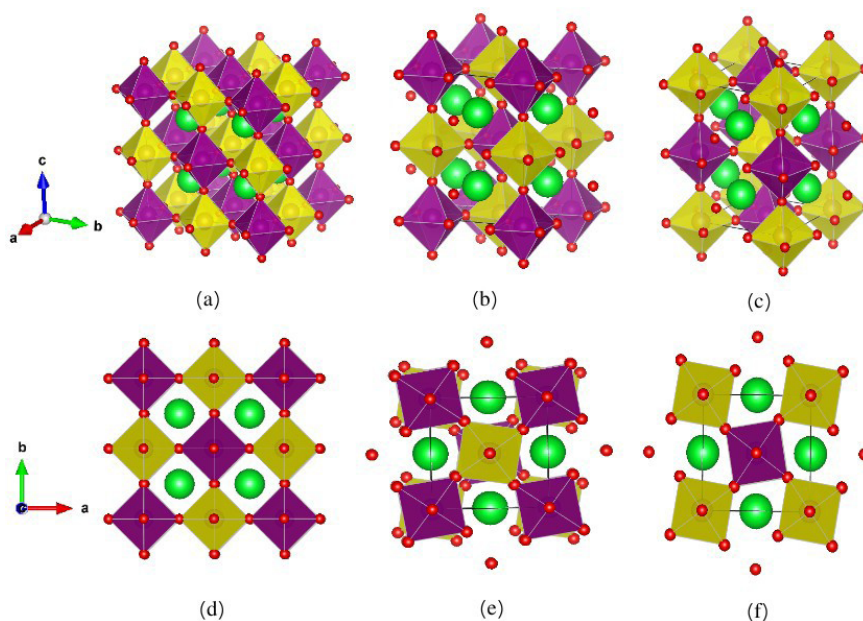
Calculations Details

DFT calculations employing the full potential linearized augmented plane wave method (FP-LAPW) were performed, such as is implemented in the WIEN2k code (Blaha *et al.*, 2001), within the spin-polarized density-functional theory framework (Khon & Sham, 1965). The exchange and correlation effects were described by the generalized gradient approximation GGA of Perdew - Burke - Ernzerhof (PBE) (Perdew *et al.*, 1996) together with the Hubbard parameter U (GGA+U). The GGA+U technique was developed during the 1990s by Anisimov and coworkers to refine DFT calculations (Anisimov *et al.*, 1991; Anisimov *et al.*, 1993;). It considers a Hubbard term for the Coulomb potential that corrects mean field interactions via an on-site (atomic) parameter, U. It was chosen the value 4.0 eV for the effective parameter U_{eff} of the d-Mn states. The iteration for self-consistency was continued until the convergence criteria, of 1×10^{-4} Ry, was reached.

The atomic positions used as input, for each space group, are shown in the **table 1**. The cubic and tetragonal supercells (Fm-3m, I4m and P4/mnc spaces group, respectively) were built using the Vesta software (Momma & Izumi, 2011), as shown in the **figure 1**. In **figure 1a**, it can be seen the crystal lattice structure for the cubic phase. In the picture it

Table 1. Atomic positions given in crystalline units, for the Fm-3m, I4m and P/4mnc phases of the Sr₂MnSbO₆ perovskite.

Space group		#225			<i>Fm-3m</i>
Element	<i>x</i>	<i>y</i>	<i>z</i>	<i>R_{MT}</i>	
Sr	0.2500	0.2500	0.2500	2,0000	
Sb	0.0000	0.0000	0.0000	2,2000	
Mn	0.5000	0.0000	0.0000	2,0000	
O	0.2504	0.0000	0.0000	1,4000	
Space group		#87			<i>I4m</i>
Element	<i>x</i>	<i>y</i>	<i>z</i>	<i>R_{MT}</i>	
Sr	0.0000	0.5000	0.2500	1,8000	
Mn	0.0000	0.0000	0.0000	2,0000	
Sb	0.5000	0.0000	0.5000	2,2000	
O1	0.0000	0.0000	0.2504	1,4000	
O2	0.2081	0.2910	0.0000	1,4000	
Space group		#128			<i>P4/mnc</i>
Element	<i>x</i>	<i>y</i>	<i>z</i>	<i>R_{MT}</i>	
Sr	0.2500	0.2500	0.2500	1,8000	
Sb	0.0000	0.0000	0.0000	2,0000	
Mn	0.5000	0.0000	0.0000	2,0000	
O1	0.2504	0.0000	0.0000	1,4000	
O2	0.2081	0.7090	0.0000	1,4000	

**Figure 1.** Crystal structures of the Sr₂MnSbO₆ perovskite. Green spheres represent Strontium atoms; Red spheres represent Oxygen atoms; The Mn³⁺ ions are shown as purple spheres in the octahedra; The Sb⁵⁺ ions are shown as yellow spheres in the octahedra. (a) Fm-3m. (b) I4m. (c) P/4mnc. (d) Top view of the Fm-3m phase. (e) Top view of the I4m phase. (f) Top view of the P/4mnc phase.

is observed the Mn³⁺ (purple spheres) and Sb⁵⁺ (yellow spheres) cations adopt octahedral correlations with its nearest neighbors, consisting of O²⁻ anions. The muffin-tin radii used were 2.0, 2.2, 2.0 and 1.4 bohr for Sr, Sb, Mn and O atoms, respectively, and a 120 k-points mesh was used in a Brillouin irreducible zone, generated according to the Monkhorst-Pack scheme (Monkhorst & Pack, 1976). The separation energy between the valence and core states was taken to be equal to -6.0 Ry, and the maximum angular momentum was $l_{\max} = 10$. The wave functions in the interstitial region were expanded in plane waves with cutoff $K_{\max} = 7.0/R_{\text{mt}}$ (where R_{mt} is the smallest muffin-tin sphere radii inside the cell).

In the case of the tetragonal I4m lattice shown in **figure 1b**, there are two atomic positions for oxygen atoms, i.e., the atoms placed in top of the octahedral site (O1) and the oxygen atoms placed on the xy-plane of the octahedron (O2), as shown in **table 1**. The muffin-tin radii used were 1.8, 2.2, 2.0 and 1.4 bohr for Sr, Sb, Mn and O atoms, respectively, and a 144 k-points mesh was used in a Brillouin irreducible zone. The separation energy between the valence and core states was taken to be equal to -6.0 Ry, and the maximum angular momentum was $l_{\max} = 10$. The wave functions in the interstitial region were expanded in plane waves with cutoff $K_{\max} = 7.0/R_{\text{mt}}$.

Similarly, **figure 1c** shows the tetragonal P/4mnc lattice. For this phase there are also two atomic positions for the oxygen atoms, axial (O1) and equatorial (O2), this is illustrated in **table 1**. The muffin-tin radii were 1.8, 2.0, 2.0 and 1.4 bohr for Sr, Sb, Mn and O atoms, respectively. A mesh of 140 k-points was used in a Brillouin irreducible zone. The separation energy between the valence and core states was taken to be equal to -8.0 Ry. As in the former cases, the maximum angular momentum was $l_{\max} = 10$ and the wave functions in the interstitial region were expanded in plane waves with cutoff $K_{\max} = 7.0/R_{\text{mt}}$.

The top view of the different phases of the compound in **figure 1** allows to better observe the arrangement of the octahedra in the different symmetries. In the cubic phase the octahedra are placed one on top of the other and the oxygen atoms are aligned with the axes, as shown in **figure 1d**. In the I4m case, the oxygen atoms are not aligned with the x- and y-axis, i.e., the octahedra present rotation around the z axis. Furthermore, the vertices of octahedra are not aligned with each other along the z axis, see **figure 1e**. The P/4mnc structure presents the same rotation of the octahedra around the z axis, as in the I4m phase, but in this case the vertices of octahedra are aligned along the z-axis, see **figure 1f**. These differences in the symmetry and arrangement of octahedra often determine the electronic behavior in compounds of this type.

Results and discussion

Structural parameters

An optimization process of the equilibrium structural parameters was performed computing the cohesive energy value of the structure for different values of the lattice constants. The energy versus volume values were fitted to the Murnaghan's equation of state (Murnaghan, 1944) with the aim to obtain the optimal structural parameters, i.e. the volume of equilibrium (V), lattice parameters of equilibrium (a and c/a ratio), bulk modulus (B) and cohesive energy (E_0). The results of the fits are shown in **table 2** which also contains some experimental values for comparison. The lattice constant obtained for the cubic phase was $a = 15.16$ bohr and the corresponding cohesive energy was -3.77 Ry. Also, for the tetragonal structure I4m, the lattice constant obtained was $a = 10.65$ bohr, the optimized ratio $c/a = 1.467$ and the cohesive energy -3.78 Ry. Furthermore, for the tetragonal P/4mnc phase, the lattice constant was 10.58 bohr, $c/a = 1.467$ and cohesive energy equal to -3.66 Ry. We highlight that the results for the lattice parameters of the cubic and I4m phases are in good agreement with the experimental values reported in (Cheah *et al.*, 2006; Ivanov *et al.*, 2009).

On the other hand, to our knowledge the only values reported for the parameters of the tetragonal P/4mnc phase are those experimentally obtained by (Parada *et al.*, 2018) which are comparable to ours, as shown in the **table 2**. In addition, it is noticed the negative value for the cohesive energy, which proves the stable character of this phase and consequently

new evidence of its existence. The energy values let us conclude that for the tetragonal symmetry, the compound prefers the arrangement shown in **figure 1e**, over the one in which the octahedra are placed in layers perfectly aligned, as shown in **figure 1f**.

Density of States (DOS)

The electronic behaviour of the compound is determined by computing and plotting the densities of states for the up and down spin polarization. Results of this for the cubic phase are shown in **figure 2**. Here, it can be seen the total density of states, along with the atomic contribution and the main contributions of the atomic orbitals. In **figure 2a**, are shown the

Tabla2. Structural parameters calculated for the Fm-3m, I4m and P4/mnc space groups of Sr₂MnSbO₆ perovskite

Fm-3m space group					
Parameter	<i>a</i> [bohr]	<i>V</i> [bohr ³]	<i>B</i> [GPa]	<i>E</i> ₀ [Ry]	
This work	15.16	871.15	155.45	-3.77	
Exp. ref. (Ivanov <i>et al.</i> , 2009)	15.0648	—	—	—	—
Exp. ref. (Cheah <i>et al.</i> , 2006)	15.0854	—	—	—	—
I4m space group					
Parameter	<i>a</i> [bohr]	<i>c/a</i> ratio	<i>V</i> [bohr ³]	<i>B</i> [GPa]	<i>E</i> ₀ [Ry]
This work	10.65	1.43	866.56	169.59	-3.78
Exp. ref. (Ivanov <i>et al.</i> , 2009)	10.4161	1.4608	—	—	—
Exp. ref. (Cheah <i>et al.</i> , 2006)	10.4526	1.4613	—	—	—
P4/mnc space group					
Parameter	<i>a</i> [bohr]	<i>c/a</i> ratio	<i>V</i> [bohr ³]	<i>B</i> [GPa]	<i>E</i> ₀ [Ry]
This work	10.58	1.46	864.47	157.24	-3.66
Exp. ref. (Parada <i>et al.</i> , 2018)	10.688	1.4180	—	—	—

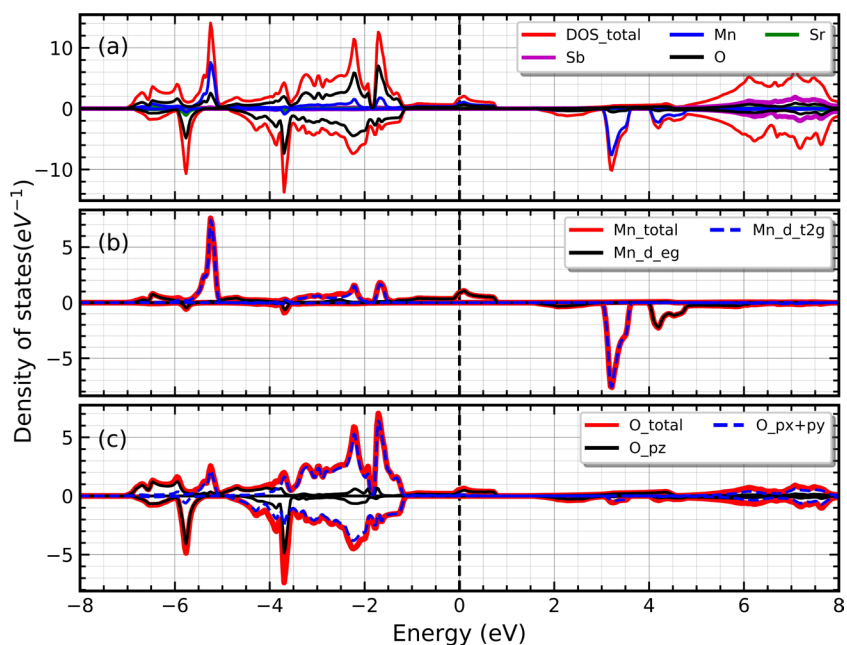


Figure 2. (a) Total density of states and atomic contribution for the cubic structure. (b) Main contribution of the Mn-atoms. (c) Main contributions of the O-atoms.

total density (red line) and the contribution of the different atomic species in the compound. The largest contribution to the density of states is due to O and Mn atoms whereas the Sr and Sb atoms does not contribute at least around the Fermi level (energy equal to zero). It is observed some states at the Fermi level corresponding to the spin up polarization whereas the spin down polarization does not present states at the Fermi level. This implies that the compound exhibits metallic-like behavior for the spin-up polarization, while in the spin-down polarization, the material behaves as semiconductor.

In addition, we can notice that the states below of Fermi level are principally due to the O atoms, in both up and down spin polarization. Some spin-up states of manganese and oxygen are present at the Fermi level while minority spin electrons are negligible indicating that the majority spin electrons alone participate in the electrical conductivity, which support the charge transportation for spin-up channel.

In **figure 2b** and **figure 2c** also are shown the partial densities of states with more considerable contribution, which are mainly due to $\text{Mn} - d$ and $\text{O} - p$ orbitals. It is easy to notice in the DOS of the $\text{Mn} - d$ orbitals, the splitting of crystalline field effects, which is due the $d - \text{Mn}$ orbitals. In a cubic transition-metal oxide crystal the transition-metal ion is in a site that has octahedral O_h symmetry and the d-levels split into threefold degenerate (lower energy) t_{2g} states and twofold degenerate (higher energy) e_g states. For the Manganese, the main contribution of t_{2g} states is about -5.2 eV while the e_g states is about the Fermi level, for the spin up density. Furthermore, it can be observed for the down polarization that t_{2g} states contribute in values about 3.2 eV and the e_g states are placed about the 4.2 eV. As demonstrated trough the values above the splitting of crystalline field for spin up polarization is more energetic than splitting for spin down polarization. The splitting of crystalline field is above 5.2 eV for up polarization and about 1.0 eV for down spin configuration. On the other hand, due to the magnetic characteristic of M cation, an exchange splitting takes place. It is observed as a difference between e_g up and down states, and a difference between t_{2g} up and down states. The splitting of exchange shows approximately 4.2 eV for high energy states and 8.4 eV for low energy states. For the oxygen atoms it is found that the $px + py$ orbitals have presence mainly in energy values less than -1.0 eV while the $\text{O}-pz$ states are also in the Fermi level.

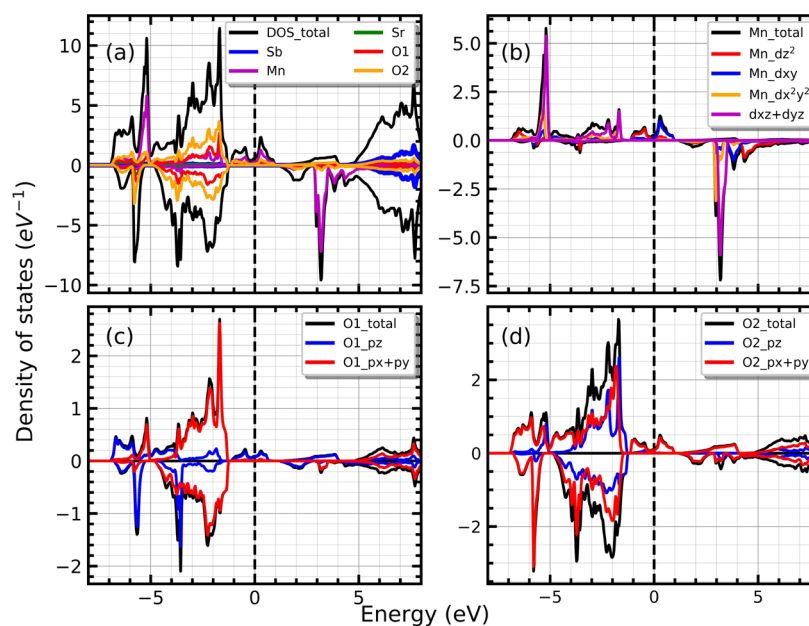


Figura 3. (a) Total density of states and atomic contribution for the tetragonal $I4m$ phase. (b) Main contribution of the Mn-atoms. (c) DOS of the O1-atoms placed at the top of octahedra. (d) Dos corresponding to the O2-atoms placed in the x-y plane of the octahedra.

The densities of states for the tetragonal I4m phase are shown in **figure 3**. The first thing to be noticed is that there are some few states about the Fermi level, corresponding to the spin up polarization. As in the cubic case, the O and Mn atoms provide states about the Fermi level while the absence of Sr and Sb states persist (see **figure 3a**). The manganese provides occupied states, mainly in the up spin polarization, which can be seen in **figure 3b**. At energies below the Fermi level, the main contribution to the DOS is due to the oxygen atoms, as shown in **figure 3c** and **figure 3d**.

In **figure 3b** the DOS for each $d - Mn$ orbitals also are shown. In this case the orbitals are not splitted in two groups as in the cubic case, due the tetragonal distortion and the oxygen-octahedron rotation. The splitting of crystal field is affected by the atomic spacing increase in the z-direction due the change to tetragonal symmetry and the arrangement of the octahedra. The so called, Jahn-Teller effect, describes this type of distortions which depends on both the strength and the symmetry of the crystal field. In this case, the bond length between the metal ion and the O1 atoms is slightly longer than the bond lengths with the O2 atoms. Also, the vertices of the octahedron are not aligned with the x- and y-axis, but rather it is rotated with respect to the z axis, as can be seen in **figure 1e**. The above destabilize the orbitals with components in the x-y plane (higher energy) and the orbitals with components along the x- and y-axis are stabilized (lower energy). The combination of the two distortions is responsible for the contributions of states near the Fermi level due the d_{z^2} and the d_{xy} orbitals, whereas the $d_{x^2+y^2}$ and d_{xz+yz} orbitals contribute at energies below the Fermi level.

The DOS for the O1 and O2 atoms are shown in **figure 3c** and **figure 3d**, respectively. In **figure 3c** it can be seen the DOS of O1 atoms, recalling that these atoms are placed at top of the octahedral site. The O1- $px + py$ states are scattered on energy values from -7.0 to -1.5 eV, in both up and down polarizations, whereas the O1- pz also are present about the Fermi level, only for spin up channel. Meanwhile, in **figure 3d** one sees that O2- pz orbitals are scattered along the energy axis from -7.0 to -1.5 eV, whereas the O2- $px + py$ orbitals also provide states about the Fermi level. So, the $Mn-d_{z^2}$, $Mn-d_{xy}$, O1- Pz and O2- $px+py$ states support the charge transport with spin up polarization. The spin down channel still behaves like a semiconductor, as in the previous case.

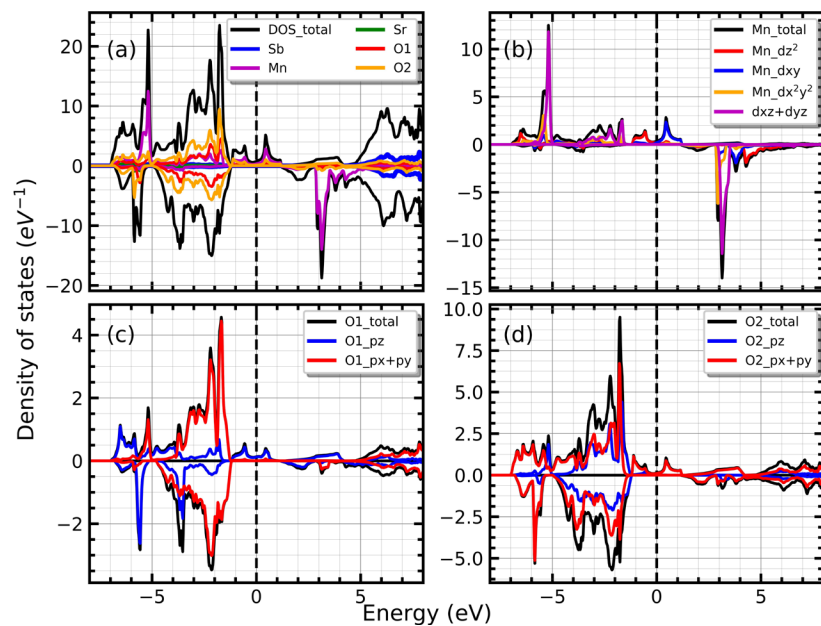


Figura 4. (a) Total density of states and atomic contribution for the tetragonal P/4mnc phase. (b) Main contribution of the Mn-atoms. (c) DOS of the O1-atoms placed at the top of octahedra. (d) Dos corresponding to the O2-atoms placed in the x-y plane of the octahedra.

Finally, let us discuss the densities of states computed for the P/4mnc phase, which are shown in the **figure 4**. It is easy to notice that the DOS for the P/4mnc are very similar to those shown in **figure 3**, for the former case. In **figure 4a**, it is observed that near the Fermi level most of the states correspond to Mn, O1 and O2 atoms. Partial densities of states showing various orbital contributions for these atoms are presented in **figure 4b**, **4c** and **4d**, respectively. Here it is possible to see that the interaction between Mn-d and O-p states produces some states about the Fermi level, appearing the metallic character in the spin up channel, while the spin down channel exhibits semiconductor behaviour. The similarity of the densities of states with the I4m phase allows us to infer that the P/4mnc phase, besides to implying the appearance of more states at the Fermi level, does not have a significant effect on the overall electronic behavior.

In all the cases studied the DOS is asymmetric with respect to the spin polarization. This asymmetrical behavior permits to obtain an effective magnetic moment. The value found was $4.0 \mu_B$ per unit cell in both Fm-3m and I4m phases, and $8.0 \mu_B$ for the P4/mnc phase.

In addition, based on the asymmetry of all the projections on the Mn orbitals, it was concluded that the magnetic moment is principally due the Mn-d orbitals contribution.

Conclusions

Theoretical calculations of density functional theory have been utilized in our study of the structural and electronic properties of the perovskite, $\text{Sr}_2\text{MnSbO}_6$. Our results are in agreement with experimental reports of structural parameters, as well as the cohesive energy and the bulk modulus are reported. Also, it is reported the p/4mnc phase whose main difference from the I4m is the arrangement of the octahedra, as shown in figure 1e and figure 1f, and as a consequence the material prefers the I4m arrangement since it has a more negative energy value (more stable) than the P/4mnc phase. The densities of states reveal a half-metallic behavior in the $\text{Sr}_2\text{MnSbO}_6$ compound, which is supported by the presence of Mn-d and O-p states about the Fermi level. Also, it is observed the asymmetric shape of the DOS with respect to the spin polarization, which implies the existence of effective magnetic moment.

Acknowledgments

Thanks to the Materials Study Group (GEMA) and the Physics of Novel Materials Group (GFNM) of the National University of Colombia (UNAL) for support this work.

Authors' contribution

JAR and JRR coordinated the work. WSC performed calculations, analyzed data and drafted the document in collaboration with L.F.M y JCO.

Conflict of interests

The authors declare that they have no conflicts of interest.

References

- Ahmad Mir, S., Gupta, D. C. (2020). Exploration of uranium double perovskites Ba_2MUO_6 (M= Co, Ni) for magnetism, spintronic and thermoelectric applications. *Journal of Magnetism and Magnetic Materials.*, 493(1), 165722.
- Anisimov, V. I., Solovyev, I. V., Korotin, M. A. (1993). Density-functional theory and NiO photoemission spectra. *Physics Review B*, 48(23), 16929-16934.
- Anisimov, V. I., Zaanen, J., Andersen, O. K. (1991) Band theory and mott insulators: Hubbard U instead of stoner I. *Physics Review B*, 44(3), 943-954.
- Antara, B., Preethi-Meher, K. R. S., Varma, K. B. R. (2011). Dielectric relaxation behaviour of $\text{Sr}_2\text{MnSbO}_6$ ceramics fabricated from nanocrystalline powders prepared by molten salt synthesis. *Bulletin of Materials Science*, 34(1), 53-60.

- Bazuev, G., Tyutyunnik, A., Gyrdasova, O., Korolevb, A.** (2021). Effect of substitutions on the phase formation, structure and magnetic properties of the double perovskites $\text{Sr}_2\text{MnSbO}_6$ and SrLaMnSbO_6 . *Journal of Magnetism and Magnetic Materials*, 543, 168624.
- Blaaha, P., Schwarz, K., Madsen, G., Kvasnicka, D., Luitz, J.** (2001). *Wien2k, an augmented plane wave plus local orbitals program for calculating crystal properties*. Vienna University of Technology.
- Bonilla, C., Landínez Téllez, D., Rodríguez, J. A., López-Vera, E., Roa-Rojas, J.** (2007). Half-metallic behavior and electronic structure of $\text{Sr}_2\text{CrMoO}_6$ magnetic system. *Physica B*, 398, 208-211.
- Cardona, R., Landínez-Téllez, D., Rodríguez M., J. A., Fajardo, F., Roa-Rojas, J.** (2008). Structural and magnetic properties of double-perovskite $\text{Ba}_2\text{MnMoO}_6$ by density functional theory. *Journal of Magnetism and Magnetic Materials*, 320.
- Cheah, M., Saines, P. J., Kennedy, B. J.** (2006). The jahn–teller distortion and cation ordering in the perovskite $\text{Sr}_2\text{MnSbO}_6$. *Journal of Solid State Chemistry*, 179(6), 1775-1781.
- Fajardo, F., Cardona, R., Landínez Téllez, D. A., Rodríguez M., J. A., Roa-Rojas, J.** (2012). Theoretical and experimental studies of structural characteristics, magnetic response and electronic properties of $\text{Sr}_2\text{FeMnO}_6$ complex perovskite. *Revista Mexicana de Física*, 58(2), 57-60.
- Foster, M. C., Nielson, R. M., Abrahams, S. C.** (1997). $\text{Sr}_2\text{MnSbO}_6$: A new semiconductor ferroelectric. *Journal of Applied Physics*, 82(6), 3076-3080.
- Ivanov, S., Nordblad, P., Tellgren, R., A., H.** (2009). Temperature evolution of structure and magnetic properties in the perovskite $\text{Sr}_2\text{MnSbO}_6$. *Materials Research Bulletin*, 44(4), 822-830.
- Khon, W., Sham, L.** (1965). Self-consistent equations including exchange and correlation effects. *Physics Review*, 140(4A).
- Liu, Y. P., Fuh, H. R., Wang, Y. K.** (2014). Expansion research on half-metallic materials in double perovskites of $\text{Sr}_2\text{BB}'\text{O}_6$ (B = Co, Cu, and Ni; B' = Mo, W, Tc, and Re; and $\text{BB}' = \text{FeTc}$). *Computational Materials Science*, 92, 63-68.
- Majhi, K., B., S.-P., Varma, K. B. R.** (2007). Dielectric relaxation behaviour of $\text{Sr}_2\text{MnSbO}_6$ ceramics. *Journal of Physics D: Applied Physics*, 40, 7128-7135.
- Mir, S. A., Gupta, D. C.** (2021). Scrutinizing the stability and exploring the dependence of thermoelectric properties on band structure of 3d-3d metal-based double perovskites $\text{Ba}_2\text{FeNiO}_6$ and $\text{Ba}_2\text{CoNiO}_6$. *Scientific Reports*, 11(1). <https://doi.org/doi: 10.1038/s41598-021-90027-7>
- Momma, K., Izumi, F.** (2011). VESTA3 for three-dimensional visualization of crystal, volumetric and morphology data. *Journal of Applied Crystallography*, 44(6), 1272-1276. <https://doi.org/10.1107/S0021889811038970>
- Monkhorst, H., Pack, J.** (1976). Special points for brillouin-zone integrations. *Physics Review B*, 13(12), 5188-5192.
- Murnaghan, F. D.** (1944). The compressibility of media under extreme pressures. *Proceedings of the National Academy of Sciences*, 30(9), 244-247.
- Ortiz-Díaz, O., Rodríguez, J. A., Fajardo, F., Landínez Te'llez, D., J., R.-R.** (2007). Electronic and structural properties of Sr_2YSbO_6 . *Physica B*, 398(2), 248–251.
- Parada, Y., Parra, C. A., Landínez-Tellez, D., Roa-Rojas, J.** (2018) Evolution of the structural ordering of the $\text{Sr}_2\text{MnSbO}_6$ perovskite as a function of temperature. *Revista de la Academia Colombiana de Ciencias Exactas, Físicas y Naturales*, 42(163), 162-165.
- Perdew, J. P., Burke, K., Ernzerhof, M.** (1996) Generalized gradient approximation made simple. *Physical Review Letters*, 77(18), 3865-3868.
- Persson, K.** (2016). *Materials data on $\text{Sr}_2\text{MnSbO}_6$ (sg:139) by materials project*. <https://doi.org/10.17188/1269777>
- Preethi-Meher, K. R. S., Janolin, P.-E., Guiblin, N., Paramesh, G., Varma, K. B. R.** (2012). High temperature phase transition studies and dielectric properties of $\text{Sr}_2\text{MnSbO}_6$. *AIP Conference Proceedings*, 1447, 137-138.
- Singh, D. J., Nordstrom, L.** (2006). Planewaves, pseudopotentials and the lapw method. United States of America: *Springer*.